Published in Applied Physics Letters 88, issue 121112, 1-3, 2006
which should be used for any reference to this work

High-quality AlN/GaN-superlattice structures for the fabrication of narrow-band 1.4 μm photovoltaic intersubband detectors

Daniel Hofstetter,[a] Esther Baumann, Fabrizio R. Giorgetta, and Marcel Graf
Institute of Physics, University of Neuchatel, 1 A.-L. Breguet, CH-2000 Neuchatel, Switzerland

Manfred Maier
Fraunhofer Institut for Applied Solid State Physics, Tullastrasse 72, D-79108 Freiburg, Germany

Fabien Guillot, Edith Bellet-Amalric, and Eva Monroy
Equipe Mixte Commissariat à l'Energie Atomique, CNRS-UJF Nanophysique et Semiconducteurs, DRFMC/SP2M/PSC, CEA-Grenoble, 38054 Grenoble Cedex 9, France

We report on high-quality short-period superlattices in the AlN/GaN material system. Thanks to significant advances in the epitaxial growth, up to 40 superlattice periods with a total layer thickness of 120 nm could be grown without cracking problems. Given an intersubband transition energy on the order of 910 meV, these superlattices could be used as room temperature, narrow-band, photovoltaic detectors for wavelengths around 1.4 μm. In photovoltaic operation, the full width at half maximum is as narrow as 90 meV, underlining the high quality of the interfaces and the single layers in our structures.

Recently, there has been increasing interest in III-nitride semiconductors for fabrication of ultrahigh-speed intersubband (ISB) devices.[1] Because of the large conduction band discontinuity of nearly 2 eV between AlN and GaN, this material combination is suitable for ISB transitions with an energy difference of roughly 1 eV.[2] Since such a large photon energy covers the technologically interesting wavelength region around 1.3/1.55 μm, passive or active modulators and photodetectors for telecommunication applications can be envisioned. It is expected that the ultrafast recovery time of such ISB transitions (150–370 fs, depending on the reference) will eventually result in high-speed devices in the $>$10 GHz range.[3,4] Shortly after the demonstration of ISB absorption in both quantum well (QW) and quantum dot superlattices (SLs),[5,6] several prototypes of QW and quantum dot ISB detectors have been published.[7–9] However, all devices reported so far, and in particular the QW-based ISB photodetectors (QWIPs), had relatively broad detection peaks [full width at half maximum (FWHM) considerably larger than 100 meV for ISB energies in the 800 meV range]. This broadening is mainly due to interfacial roughness and might be augmented by drift of the growth rate during the epitaxy. Recently, improved deposition techniques based on the use of In as a surfactant during epitaxial growth of AlGaN, GaN, and AlN layers have resulted in significantly smoother surfaces, and therefore a better interface quality.[10]

In this letter, we present a series of QWIP samples with a nominally identical active region, i.e., the same QW and barrier layer thickness, and differing in the doping level in the QWs and the thickness of the cap layer only. All samples present extremely narrow (FWHM ~90 meV) TM-polarized absorption/detection spectra at an ISB transition wavelength around 1.4 μm, which demonstrates both improved crystalline quality of the layers and interfaces and high reproducibility of the growth process.

[a]Electronic mail: Daniel.Hofstetter@unine.ch

QWIP structures consist of 40 periods of 1.0-nm-thick Si-doped GaN QWs with 2.0-nm-thick AlN barriers, grown by plasma-assisted molecular-beam epitaxy (PAMBE) on 1-μm-thick AlN-on-sapphire substrates. Active nitrogen was provided by a radio-frequency plasma cell, and standard effusion cells were used for Ga, Al, Si, and In. The doping level in the GaN QWs was 5×10^{19} cm^{-3} for sample E728 and 1×10^{19} cm^{-3} for E739 and E740. Prior to the growth of the active region, a 250-nm-thick Si-doped $Al_{0.65}Ga_{0.65}N$ buffer layer was deposited. On top of the active region, we deposited a Si-doped $Al_{0.65}Ga_{0.65}N$ cap layer with a thickness of 5 nm (sample E740) or 180 nm (samples E728 and E739). The idea behind the variations between the different samples was to have, in three otherwise identical structures, one heavily doped reference sample for direct multipass-absorption measurements (E728), and two moderately doped samples (E739 and E740) for electromodulated absorption and photodetector measurements, respectively.

The choice of $Al_{0.65}Ga_{0.65}N$:Si as a cladding layer aims to fabricate devices whose average Al content in the cladding layer matches the average Al content of the active region. This design is advisable in order to reduce the defects along the active region, and to prevent a gradient in the internal electric field due to spontaneous and piezoelectric polarization. However, the structural quality of AlGaN alloys is often one of the limitations in the performance of nitride-based devices. The difficulty in the growth of AlGaN lies in the strength of the Al-N bond, which results in a reduction of the surface mobility of Al as compared to Ga species in PAMBE. Nevertheless, the growth of AlGaN layers with an Al mole fraction smaller than 35% can be performed under Ga-rich conditions without deterioration of the surface morphology or crystalline quality. However, when increasing the Al mole fraction to values higher than 50%, we observe a significant enhancement of the surface roughness, to typical rms values of ~4 nm on a surface of 5×5 μm^2.

In a previous work, we have demonstrated the capability of In as a surfactant for AlGaN growth, delimiting the range of substrate temperatures and In fluxes at which an In adlayer

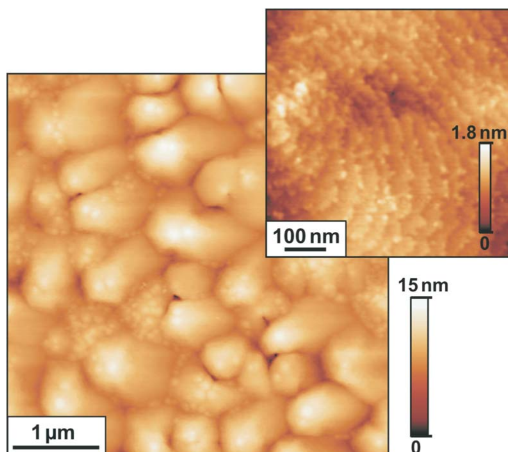

FIG. 1. (Color online) AFM surface scans of the SL sample E740 that was grown on a 65% AlGaN buffer. The rms roughness on the 5×5 μm^2 area shown is 1.7 nm. In the zoomed image, we observe atomic-step terraces otherwise typical for the growth of GaN, indicating a short-range roughness at the monolayer scale.

is dynamically stable on $Al_xGa_{1-x}N(0001)$.[9] In the present work, we have applied this growth procedure to QWIP structures. The surface morphology of the samples was analyzed by atomic force microscopy (AFM) in the tapping mode, using a Dimension 3100 system. Figure 1 presents an AFM scan of sample E740: on an area of 5×5 μm^2, it shows an rms surface roughness of about 1.7 nm. In the zoomed image of Fig. 1, we observe atomic-step terraces typical for the growth of GaN; they indicate a short-range roughness at the monolayer scale.

The structural quality of the SLs has been further assessed by high-resolution x-ray diffraction (HRXRD) measurements using a SEIFERT XRD 3003 PTS-HR diffractometer with a beam concentrator prior to the Ge(220) four-bounce monochromator and a Ge(220) two-bounce analyzer in front of the detector. HRXRD (ω-2θ) scans of the (0002) x-ray reflection of all three wafers are shown in Fig. 2(a). First, they reveal excellent reproducibility of the growth process. Second, from simulations of the ω-2θ scan of the (0002) reflection [shown in Fig. 2(a)], and of the (10−15)

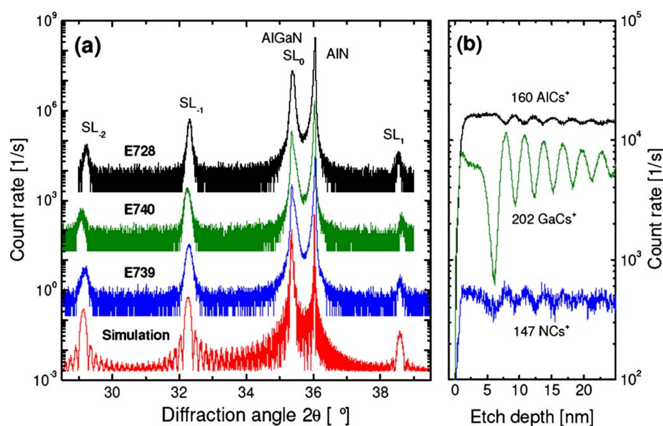

FIG. 2. (Color online) (a) HRXRD ω-2θ scans of the (0002) reflection of samples E728, E739, and E740. The simulation was performed using the program X'PERT EPITAXY 40 from Phillips Analytical, assuming that the structure is fully strained on the AlN buffer. (b) SIMS measurements on sample E740. $AlCs^+$, $GaCs^+$, and NCs^+ signals as a function of depth are shown. The depth calibration could be based on the SL period of 2.93±0.04 nm as determined by HRXRD.

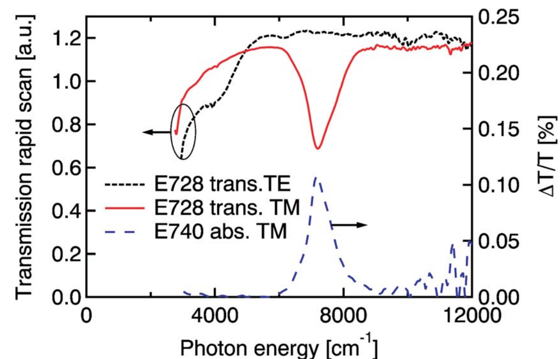

FIG. 3. (Color online) Direct absorption measurements in TE (short dashed line) and TM polarization (solid line) of E728 and TM-polarized electromodulated absorption spectrum (long dashed line) of E740. The features at 3000 cm^{-1} on the low energy side are artifacts due to the normalization with a reference spectrum that approaches zero in that wavelength range.

reciprocal space map, we verified that the average Al mole fraction of the claddings matches the average Al content of the SL (overlapping peaks for $Al_{0.65}Ga_{0.65}N$ and the zeroth order of the SL), and we conclude that the whole structure is strained on the AlN buffer layer. Third, despite the extremely small SL period, we observe SL satellite peaks up to the second order, confirming an average period of 2.93±0.04 nm.

As a final indication for the excellent material quality, we show in Fig. 2(b) secondary ion mass spectroscopy (SIMS) measurements of sample E740. The profiles were measured by using a 500 eV Cs^+ primary ion beam and under a very shallow incidence angle (67.5° to the normal). One can see the periodicities of the secondary $AlCs^+$ (160 a.u.) and NCs^+ (147 a.u.) signals, which correlate well with the much more pronounced periodicity of the secondary signal from $GaCs^+$ ions (202 a.u.). The depth calibration was based on the results from the previous x-ray diffraction experiment.

By using a self-consistent Schrödinger-Poisson equation solver, we were able to compute the energy levels in such a SL. This simulation predicted a transition energy of about 880 meV. Since many-body effects were not yet taken into account, this value has an error bar of roughly ±100 meV. From now on, experiments concentrated on samples E728 and E740. For the direct absorption experiment, we polished sample E728 in a standard multipass geometry with a mirrorlike back and two parallel 45° wedges.[7] Absorption was then measured by passing white light from a Fourier transform infrared spectrometer through the sample. Measuring first the TM- and then the TE-polarized sample transmission and background spectra allowed us to obtain normalized absorption signals, I_{TE} and I_{TM}, which are shown in Fig. 3 (I_{TE}: short-dashed line; I_{TM}: solid line). Based on Fermi's golden rule, we compared the experimentally observed absorbance signal, $\ln(I_{TE}/I_{TM})=\alpha\times L=0.44$, with the computed value of $\alpha\times L=0.53$ using a dipole matrix element of the transition of $\langle 1|z|2\rangle=2.5$ Å, a sheet carrier density of $n_s=7.5\times10^{12}$ cm^{-2}, and a number of passes times the number of wells, $n_{tot}=10\times40=400$, and observed good agreement.

For the five times lower doped sample E740 we used: a more sensitive measurement technique, namely electromodulated absorption. Sample preparation in this case relied on polishing of a multipass waveguide as well. At the sample

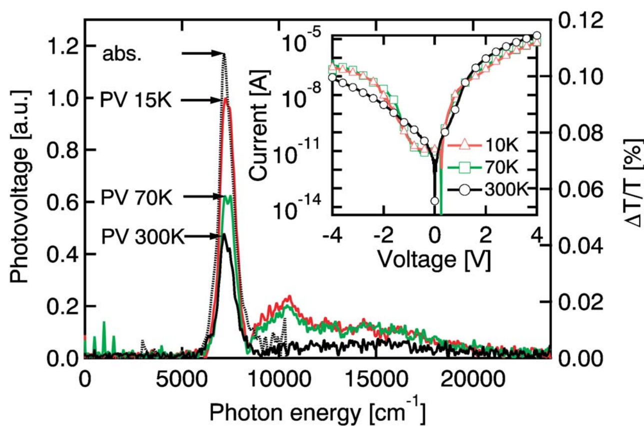

FIG. 4. (Color online) Photovoltage measurements on sample E740 in TM polarization for 15, 70, and 300 K. Although the signal decreases at higher temperatures, it is still well visible at room temperature. Note the good agreement with the absorbance spectra shown as a dotted line. The inset shows the *I-V* characteristics of the Schottky diode at three representative temperatures.

surface, however, we added two Ohmic contacts and one Schottky contact stripe. The Cr/Au (10/400 nm) Ohmic contacts measure 0.5×3 mm^2 (their length corresponds to the distance between the two parallel 45° facets), and they are separated by 3 mm. In between, we evaporated an identically large stripe of the same contact metals, but this time on top of a 50-nm-thick SiO_2 layer instead of the bare semiconductor. *I-V* characteristics of the resulting Schottky diode are shown in the inset of Fig. 4. During the electromodulated absorption experiment, rectangularly shaped voltage pulses at a duty cycle of 50%, a repetition frequency of 13 kHz, and a height of −2 V were applied between the Schottky and Ohmic contacts. The resulting electric field under the Schottky contact periodically depleted the electron concentration in the top wells, inducing a measurable transmission change. Thanks to the periodic nature of the depletion and enhancement, a synchronous detection setup could be used to increase the sensitivity. With such an arrangement, it is therefore possible to resolve transmission or absorption changes on the order of $\Delta T/T = 10^{-4}$.[11] The spectrum of such a measurement, normalized by division with the corresponding rapid scan transmission spectrum through the sample, is shown in Fig. 3 (long-dashed line). Although E728 and E740 have a factor of 5 different doping concentrations, and despite the fact that they have been fabricated 12 growth runs apart from each other, we note that their absorbance spectra agree almost perfectly. Given the fact that E740 has a 5 times lower doping level but a 400 times smaller maximum absorbance than E728, we estimate that only the first QW should have seen the externally applied field. Of course, a complete depletion of a QW is probably not a very realistic scenario, so that eventually the top two or three wells might have been influenced by the electric field. Finally, when having a small drift during SL growth, probing only two or three out of 40 QWs could easily explain a smaller spectral linewidth of the electromodulated absorption spectrum.

In both direct multipass absorption and electromodulated absorption experiments, the absorbance peaks at 7280 cm^{-1} (910 meV, 1.4 μm). The FWHM of the direct absorption is 880 cm^{-1} (110 meV), whereas the electromodulated absorption has a slightly smaller width of 780 cm^{-1} (98 meV) $[(\Delta\nu/\nu)^{-1} = 9.3]$.

Figure 4 presents the characterization of E740 as photovoltaic ISB photodetector. In this experiment, the sample was illuminated by the white light source of the Fourier spectrometer. Similar to the results described earlier in Ref. 8, the Schottky contact leads to a band bending at the sample surface and thus a (somewhat inefficient) transport of electrons to the top of the SL under illumination. The resulting electron accumulation under the Schottky contact results in a small photovoltage, which was amplified and fed back into the external detector port of the spectrometer. This photovoltage, which can be seen up to room temperature, is shown in Fig. 4 for three representative temperatures. Again, a very good agreement between the photovoltage signal and the absorbance peaks is evident. The photovoltage at 10 K peaks at 7320 cm^{-1} (915 meV, 1.39 μm) and has a width of 720 cm^{-1} (90 meV) $[(\Delta\nu/\nu)^{-1} = 10.2]$. At the high energy side of the ISB signal, a broad impurity related band shows up (at an energy of about 9500 cm^{-1}), especially at high temperatures.[12]

In conclusion, we have characterized three different PAMBE-grown QWIP structures with AlN/GaN SLs grown on AlGaN claddings, where the Al mole fraction of the cladding matches the average Al content of the active region. Improved material quality is achieved by using In as a surfactant during growth, as confirmed by all structural investigations. Finally, temperature-dependent photovoltage measurements revealed a surprisingly narrow detection peak that was again fully compatible with the observed absorbance spectra. All these facts, together with the reproducibility of the results, prove that nitride PAMBE has reached a high degree of maturity.

The authors acknowledge the financial support of the Professorship Program and the National Center of Competence in Research "Quantum Photonics," sponsored by both the Swiss National Science Foundation, and the European STReP NITWAVE, Contract no. 004170.

[1] J. Hamazaki, S. Matsui, H. Kunugita, K. Ema, H. Kanazawa, T. Tachibana, A. Kikuchi, and K. Kishino, Appl. Phys. Lett. **84**, 1102 (2004).
[2] O. Ambacher, B. Foutz, J. Smart, J. R. Shealy, N. G. Weimann, K. Chu, M. Murphy, A. J. Sierakowski, W. J. Schaff, L. F. Eastman, R. Dimitrov, A. Mitchell, and M. Stutzmann, J. Appl. Phys. **87**, 334 (2000).
[3] N. Iizuka, K. Kaneko, N. Suzuki, T. Asano, S. Noda, and O. Wada, Appl. Phys. Lett. **77**, 648 (2000).
[4] C. Gmachl, S. V. Frolov, H. M. Ng, S.-N. G. Chu, and A. Y. Cho, Electron. Lett. **37**, 378 (2001).
[5] C. Gmachl, H. M. Ng, and A. Y. Cho, Appl. Phys. Lett. **79**, 1590 (2001).
[6] K. Moumanis, A. Helman, F. Fossard, M. Tchernycheva, A. Lusson, F. H. Julien, B. Damilano, N. Grandjean, and J. Massies, Appl. Phys. Lett. **82**, 868 (2003).
[7] D. Hofstetter, S.-S. Schad, H. Wu, W. J. Schaff, and L. F. Eastman, Appl. Phys. Lett. **83**, 572 (2003).
[8] E. Baumann, F. R. Giorgetta, D. Hofstetter, H. Lu, X. Chen, W. J. Schaff, L. F. Eastman, S. Golka, W. Schrenk, and G. Strasser, Appl. Phys. Lett. **87**, 191102 (2005).
[9] L. Doyennette, L. Nevou, M. Tchernycheva, A. Lupu, F. Guillot, E. Monroy, R. Colombelli, and F. H. Julien, Electron. Lett. **41**, 1077 (2005).
[10] E. Monroy, B. Daudin, E. Bellet-Amalric, N. Gogneau, D. Jalabert, F. Enjalbert, J. Brault, J. Barjon, and L. S. Dang, J. Appl. Phys. **93**, 1550 (2003).
[11] J. Faist, F. Capasso, C. Sirtori, D. L. Sivco, A. L. Hutchinson, S. N. G. Chu, and A. Y. Cho, Appl. Phys. Lett. **65**, 94 (1994).
[12] V. Ursaki, I. Tiginyanu, P. Ricci, A. Anedda, S. Hubbard, and D. Pavlidis, J. Appl. Phys. **94**, 3875 (2003).